NASA Technical Memorandum 106579

Validation of the RPLUS3D Code for Supersonic Inlet Applications Involving Three-Dimensional Shock Wave-Boundary Layer Interactions

Kamlesh Kapoor, Bernhard H. Anderson,
and Robert J. Shaw
Lewis Research Center
Cleveland, Ohio

September 1994

National Aeronautics and
Space Administration

VALIDATION OF THE RPLUS3D CODE FOR SUPERSONIC INLET APPLICATIONS INVOLVING THREE-DIMENSIONAL SHOCK WAVE-BOUNDARY LAYER INTERACTIONS

Kamlesh Kapoor,* Bernhard H. Anderson, and Robert J. Shaw
National Aeronautics and Space Administration
Lewis Research Center
Cleveland, Ohio 44135

SUMMARY

A three-dimensional computational fluid dynamics code, RPLUS3D, which was developed for the reactive propulsive flows of ramjets and scramjets, was validated for glancing shock wave-boundary layer interactions. Both laminar and turbulent flows were studied. A supersonic flow over a wedge mounted on a flat plate was numerically simulated. For the laminar case, the static pressure distribution, velocity vectors, and particle traces on the flat plate were obtained. For turbulent flow, both the Baldwin-Lomax and Chien two-equation turbulent models were used. The static pressure distributions, pitot pressure, and yaw angle profiles were computed. In addition, the velocity vectors and particle traces on the flat plate were also obtained from the computed solution. Overall, the computed results for both laminar and turbulent cases compared very well with the experimentally obtained data.

INTRODUCTION

The problem of a three-dimensional shock wave-boundary layer interaction has received extensive attention over the past 20 years because of its practical importance in a wide variety of aerodynamic problems. Common examples are the interactions in high-speed aircraft inlets, transonic compressors, wing-fuselage junctions, and control surfaces. A glancing interaction is one of the most important types of three-dimensional interactions, in that an oblique shock wave generated by one body crosses the path of a boundary layer growing along an adjacent wall. There are various kinds of glancing shock wave problems, some of which deal with complex geometries; however, the present work focuses on the problem of a supersonic flow over a wedge mounted on a flat plate, as shown in figure 1. This simple geometry represents the interaction of the shock wave generated by the wedge and a boundary layer growing on the side walls of rectangular supersonic inlets.

This report considers the interaction of a glancing shock wave with laminar and with turbulent boundary layers. Because a glancing shock wave interaction involves both shock waves and flow separation—two of the most difficult features to accurately predict numerically—it presents one of the most difficult problems for any compressible Navier-Stokes solver. Since laminar interactions do not involve the uncertainties of turbulent modeling, they are better test cases. The problem of a supersonic flow over a wedge mounted on a flat plate has been studied both experimentally and computationally by many investigators (refs.1 to 14). The objective of the present study was to assess the accuracy of the RPLUS3D code in modeling a three-dimensional shock wave-boundary layer interaction such as those which often occur in rectangular supersonic aircraft inlets. The Baldwin-Lomax (ref. 15) and Chien two-equation (ref. 16) turbulence models were used for the turbulent case.

The RPLUS3D code was used to solve the full three-dimensional Reynolds-averaged Navier-Stokes equations, and the results were compared with available experimental and computational results. For the laminar case, computations were performed for $M_o = 2.25$, $\alpha = 6°$, and $Re_L = 1.08 \times 10^5$. The results were compared with the experimental data of Degrez and Ginoux (ref. 1) and also with the numerical results of Hung (ref. 2) and

*National Research Council—NASA Research Associate at NASA Lewis Research Center.

Degrez (ref. 3). The turbulent case computations were carried out for $M_o = 2.94$, $\alpha = 10°$, and $Re_{\delta_o} = 9.25 \times 10^5$, and the results were compared with the experimental data of Oskam et al. (ref. 4).

SYMBOLS

L	characteristic length used to calculate Reynolds number (distance from flat plate leading edge to wedge apex)
M	Mach number
p	static pressure
Pt	pitot pressure
Re	Reynolds number
t	temperature
x, y, z	Cartesian coordinates
$\Delta x, \Delta y, \Delta z$	grid spacings in x-, y-, and z-directions
yg	y distance from the wedge
α	wedge angle
β	yaw angle
δ	boundary layer thickness

Subscripts:

L	based on characteristic length
o	tunnel free-stream condition
δ	based on boundary layer thickness

RPLUS3D CODE

The RPLUS3D code was developed to study mixing and chemical reaction in the flowfield of ramjets and scramjets (refs. 17 and 18). It employs an implicit finite volume, lower-upper symmetric successive overrelaxation (LU-SSOR) scheme to solve the full three-dimensional Reynolds-averaged Navier-Stokes equations and species transport equations in a fully coupled manner. Yoon and Jameson (refs. 19 and 20) initially developed the LU-SSOR scheme for nonreacting flows; after extensive testing, they showed that it was very robust and efficient for transonic and supersonic flows. We feel that the RPLUS3D code has the potential to provide a substantial speed advantage over existing Navier-Stokes codes.

A switching parameter in the RPLUS3D code allows it to be used for either a reacting or nonreacting flow. In this study, air was treated as a single species, nonreacting gas.

Laminar Case

Experimental background.—Degrez and Ginoux (ref. 1) conducted an experimental investigation of a three-dimensional oblique shock wave-laminar boundary layer interaction. The experiments were performed in a supersonic wind tunnel at the von Karman Institute. This is a continuous, closed-circuit facility with a 40- by 40-cm^2 (16- by 16-$in.^2$) test section. The free-stream Mach number was 2.25, and the test models were at near-adiabatic wall temperature for all tests. The incoming boundary layer to the flat plate was two dimensional and laminar. A series of oblique shock waves were generated by wedges at angles α of 4°, 6°, and 8° with respect to the free-stream flow direction. The wedges could be fixed on the flat plate at three different longitudinal stations, which resulted in boundary layer thicknesses of 0.11 to 0.22 cm (0.043 to 0.087 in.) and unit Reynolds numbers of 1.2×10^6 to 2.4×10^6/m. The Reynolds number based on the boundary layer thickness δ at the location of the apex varied between 1800 and 3600. The width of the plate spanned the tunnel. The experimental data consisted of surface static pressures and surface flow visualization. Details of the experiments can be found in reference 1.

Numerical Procedure.—The grid and boundary conditions used for the computational analysis are presented herein.

Grid: Figure 2 shows the physical domain and grid system used in the present study. The apex of the wedge was placed (see fig. 1) at a distance L = 9 cm (3.54 in.) from the flat plate leading edge, and the distance L was used as the characteristic length. The domain of the computation was defined by $-1.0 \le x/L \ge 3.5$, $0.0 \le y/L \ge 4.5$, and $0.0 \le z/L \ge 1.5$. In the present study, three different grids were employed. The coarse grid had 61 by 45 by 45 mesh points and was uniform in the streamwise direction and geometrically stretched in the y- and z-directions. The medium grid had the same number of mesh points as the coarse mesh, but it had additional geometric stretching in the streamwise direction from the apex of the wedge. The fine grid had 91 by 61 by 61 mesh points, and it was geometrically stretched like the medium grid.

Boundary conditions: The physical domain of the grid is shown in figure 2. On the solid surfaces (ABCDEF and CDMK) a no-slip adiabatic boundary condition was specified. Along the plane of symmetry (BCKJ), a symmetric boundary condition was used. On the outer (AFEGHI) and upper (IJKMGH) surfaces, a slip boundary condition was specified. At the upstream boundary, a few mesh points ahead of the flat plate leading edge, a uniform and supersonic free-stream flow condition was assumed (M_o, t_o, and p_o were specified). On the downstream boundary (DEGM), an extrapolation boundary condition was used.

The initial condition for the governing equations was obtained by setting all the flow variables throughout the domain equal to the inflow conditions. The computations were performed on the Cray-YMP computer at NASA Lewis Research Center. The code required 2.6 hr of CPU time to achieve global convergence for the coarse and medium grids, and 6.8 hr for the fine grid.

Results and discussion.—Our computational results were compared with the experimental data of Degrez (ref. 1) and the computational results of Hung (ref. 2) and Degrez (ref. 3) for M_o = 2.25, α = 6°, and $Re_L = 1.08\times10^5$.

Figure 3 shows the computed three-dimensional static pressure distribution on the flat plate for the fine grid solution. The pressure rise along the leading edge of the flat plate is due to the leading edge shock. The surface pressures then drop almost to the free-stream value. The pressures start rising again because of the presence of

an oblique shock wave on the flat plate. This pressure rise is followed by a sharp plateau, which represents the flow separation on the flat plate. The pressures reach their peak value, which represents the reattachment of flow on the flat plate, and then they gradually decrease.

Figure 4 shows a comparison of surface pressures at y = 5 cm (1.97 in.). Our computations, in general, are in good agreement with the experimental data of Degrez (ref. 1) and the computational results of Hung (ref. 2). The computational results of Degrez (ref. 3), however, show a prominent dip after the separation. This dip after the pressure plateau indicates a secondary flow separation. Our computations show a slight dip after the separation, which becomes more prominent for the medium- and fine-grid solutions. The results of the fine-grid solution appear to be closer to Hung's computational results, except near the separation point.

It is interesting to note that none of the computed results were able to match the experimental data after the flow reattachment; the computational results show a modest decrease in pressure, whereas the experimental data show a considerable drop in the pressure measurements. This difference is a result of the experiments being performed with a wedge of finite length, which produced an expansion fan behind the shock wave. The effect of the expansion fan influenced the upstream pressure distribution on the flat plate and caused a decrease in the measured pressure distribution. The computations were not designed to include numerical simulation of the expansion fan.

Figure 5(a) shows the fine-grid computed velocity vectors on the flat plate. The velocity vectors show the incoming stream lines converging to form a line along which the flow separates from the flat plate. This convergence line is also called the coalescence line. Farther downstream, the stream lines diverge along a line called the divergence line. The divergence line is characteristic of a reattaching flow. The figure also shows approximate positions of the coalescence line, divergence line, and inviscid shock wave. Between the coalescence line, where the flow separates, and the divergence line, where the flow reattaches, supersonic vortical flow occurs. This is characteristic of the glancing shock wave-boundary layer interaction.

Figure 5(b) shows the surface particle traces on the flat plate for the fine-grid solution. The numerical particle trace was constructed by a time integration of velocity components restricted to the second plane above the flat plate. These particle traces are considered to be equivalent to oil flow visualization in the experiment. Approximate positions of the coalescence (separation) line, divergence (reattachment) line, and inviscid shock are also marked in the figure.

Turbulent Case

Experimental background.—Figure 6 shows the schematic diagram of the experimental configuration of Oskam et al. (ref. 4). A 10° wedge was mounted on the side wall of a 20- by 20-cm (8- by 8-in.) supersonic wind tunnel. The nominal free-stream Mach number was 2.94, and the free-stream Reynolds number was 6.75×10^7/m. No details of the incoming boundary layer were provided in reference 4, other than that the boundary layer height was approximately 1.37 cm. The Reynolds number based on the boundary layer thickness δ_o was 9.25×10^5. Oskam measured static pressure distributions, pitot pressure profiles, and yaw angle profiles on the flat plate (wind tunnel floor). The locations of the data stations for α = 10° are shown in figure 7.

Numerical procedure.—The grid and boundary conditions used for the computational analysis are presented herein.

Grid: Half of the wind tunnel was numerically simulated in our computations. A computational grid of 81 by 41 by 41 was used in this study. The streamwise grid spacing Δx was uniform, and equal to $0.37\delta_o$, but the grid spacing in cross plane was geometrically stretched from the solid walls. The maximum grid spacing in

the y-direction ($\Delta y/\delta_o$) was 1.03, and in the z-direction ($\Delta z/\delta_o$) was 0.52. The typical number of grid points within the boundary layer was 22 for the flat plate.

Boundary conditions: The boundary conditions used for the turbulent case were similar to those used for the laminar case, except that a computed boundary layer profile was specified at the entrance. Since no details were provided on the incoming boundary layer profile for the Oskam experiment, a boundary layer profile was approximated by calculating the development of a turbulent boundary layer in a square duct to the point where the boundary layer thickness was equal to the experimental value. The computations were performed on the CRAY-YMP supercomputer at NASA Lewis. The code required 6.75 hr of CPU time to achieve global convergence.

Results and discussion.—Figure 8 presents comparisons of the computed and the experimental static pressure distributions on the flat plate at four different streamwise locations. The static pressure distribution on the flat plate is shown as a function of y-distance from the wedge (yg) at a specified x-distance from the wedge leading edge.

Figure 8(a) shows the static pressure distribution on the flat plate at x = 12.95 cm (5.1 in.). The pressure increases from a free-stream value of one at 16 cm from the wedge to a value of nearly two at the wedge surface. As expected, the pressure increases gradually across the shock wave. The location of the shock wave as determined from the experiment is also shown in the figure. The agreement between the computed result and the experimental data is generally good. The Chien two-equation model gives results that more closely match the experimental data than does the Baldwin-Lomax model.

The static pressure distributions for x = 18.03 cm (7.1 in.), 20.57 cm (8.1 in.), and 23.11 cm (9.1 in.) are shown in figure 8 parts (b) to (d), respectively. Here, the agreement between computed and experimental results is best at x = 12.95 cm and worst at x = 23.11 cm.

Figure 9 presents comparisons of the computed and experimentally measured pitot pressure profiles at the flat plate. Figure 9(a) shows a pitot pressure profile normal to the plate at x = 9.14 cm (3.6 in.) and yg = 6.07 cm (2.4 in.). This location is upstream of the inviscid shock location and represents an inflow condition to the interaction. The computed profiles compare fairly well with experimental data; however, they slightly overpredict the boundary layer thickness. The Baldwin-Lomax and Chien two-equation turbulent models predict nearly the same results. Parts (b) and (c) of figure 9 show pitot pressure profiles for x = 9.14 cm (3.6 in.) at yg values of 7.37 cm (2.9 in.) and 9.91 cm (3.9 in.), respectively.

Figure 9(d) presents the pitot pressure profiles at x = 18.03 cm (7.1 in.) and yg = 1.91 cm (0.75 in.). This rake location is far downstream of the inviscid shock location and represents an outflow condition from the interaction. The experimentally determined profile is somewhat similar to a turbulent boundary layer profile, except near the wall where it resembles a boundary layer profile in the vicinity of flow separation. The computations predicted this feature, but not the rest of the boundary layer profile.

Figure 9(e) shows the pitot pressure profile at x = 18.03 cm (7.1 in.) and yg = 3.18 cm (1.25 in.). Both the experimental and calculated results show trends similar to those in figure 9(d).

The differences between the calculated and experimental results may be due to (1) the use of a calculated boundary layer profile since the experiment's incoming boundary layer profile was not available; and (2) the use of a relatively coarse grid in the calculations (Reddy and Harloff (ref. 13) reported that results could be improved by using a finer grid).

Figure 10 presents yaw angles at x = 18.03 cm (7.1 in.) for yg equal to (a) 0.64 cm (0.25 in.); (b) 1.91 cm (0.75 in.); and (c) 3.18 cm (1.25 in.). The yaw angles are plotted as a function of the vertical distance z above the flat plate. Considering the curve from left to right, one moves from the flat plate toward the external flow. In the external flow, the yaw angle is approximately 10°, corresponding to the wedge angle and inviscid shock wave. The yaw angle decreases away from the plate, with a break in the curve near the edge of the boundary layer. The agreement between the results from experiments and computations is excellent. Both the Baldwin-Lomax and Chien two-equation turbulent models performed very well.

Figure 11 shows the computed velocity vectors and particle traces on the flat plate for turbulent flow, as determined with the Baldwin-Lomax turbulence model. Qualitatively, the results are similar to those for the laminar flow as presented in figure 5.

CONCLUDING REMARKS

The RPLUS3D code was validated for a glancing shock wave-boundary layer interaction by numerically simulating a supersonic flow over a wedge mounted on a flat plate. Both laminar and turbulent flow cases were examined.

For laminar flow, the static pressure distribution, velocity vectors, and particle traces on the flat plate were obtained. The computed static pressure distributions were found to be in good agreement with the available experimentally determined results.

For the turbulent case, the Baldwin-Lomax and Chien two-equation turbulent models were used to compute the surface static pressure distributions, pitot pressure, and yaw angle profiles. These were then compared with the corresponding experimental data. Overall, the computed results compared very well with those from the experiments. The Chien two-equation turbulence model performed better than the Baldwin-Lomax model.

ACKNOWLEDGMENT

Thanks are due to Dr. Jinho Lee of Sverdrup Technology Inc., NASA Lewis Research Center Group for making the RPLUS3D code available and for useful discussions regarding this work.

REFERENCES

1. Degrez, G.; and Ginoux, J.J.: Surface Phenomena in a Three-Dimensional Skewed Shock Wave/Laminar Boundary Layer Interaction, AIAA J., Vol. 22, No. 12, Dec. 1984, pp. 1764–1769.

2. Hung, C.M.: Simulation of Glancing Shock Wave and Boundary Layer Interaction, NASA TM–102233, Oct. 1989.

3. Degrez, G.: Computation of a Three-Dimensional Skewed Shock Wave Laminar Boundary Layer Interaction. AIAA Paper 85–1565, July 1985.

4. Oskam, B.; Vas, I.E.; and Bogdonoff, S.M.: Mach 3.0 Oblique Shock Wave/Turbulent Boundary Layer Interaction in Three-Dimensions. AIAA Paper 76–336.

5. Hung, C.M.; and MacCormack, R.W.: Numerical Solution of Three Dimensional Shock Wave and Turbulent Boundary Layer Interaction. AIAA J., Vol. 16, No. 12, Dec. 1978, pp. 1090–1096.

6. Kubota, H.; and Stollery, J.: An Experimental Study of the Interactions Between a Glancing Shock Wave and a Turbulent Boundary Layer, J. of Fluid Mech., Vol. 116, March 1982, pp.431–458.

7. Anderson, B.H.; and Benson, T.J.: Numerical Solution to the Glancing Sidewall Oblique Shock Wave/ Turbulent Boundary Layer Interaction in Three-Dimensions. AIAA Paper 83–0136. Jan. 1983.

8. Knight, D.D.: Calculation of Three Dimensional Shock Turbulent Boundary Layer Interaction Generated by Sharp Fin, AIAA J., Vol. 23, No. 12, Dec. 1985, pp. 1885–1891.

9. Horstman, C.: Computation of Sharp Fin Induced Shock/Boundary Layer Interactions, AIAA Paper 86–1032, May 1986.

10. Knight, D.D. et al.: Structure of Supersonic Turbulent Flow Past a Sharp Fin. AIAA J., Vol. 25, No. 10, Oct. 1987, pp. 1331–1337.

11. Aso, S.; Hayashi, M.; and Tan, A.Z.: The Structure of Aerodynamic Heating in Three-Dimensional Shock Wave/Turbulent Boundary Layer Induced by Sharp and Blunt Fins. AIAA Paper 89–1854, June 1989.

12. Knight, D.; Horstman, C.; and Settles, G.: Three-Dimensional Shock Wave-Turbulent Boundary Layer Interactions Generated by a Sharp Fin at Mach 4. AIAA Paper 91–0648.

13. Reddy, D.R.; and Harloff, G.J.: Three-Dimensional Viscous Flow Computations of High Area Ratio Nozzles for Hypersonic Propulsion. J. of Propul. and Power, Vol. 7, Jan.-Feb. 1991, pp. 84–89.

14. AGARD-AR-270: Air Intakes for High Speed Vehicles. Sept. 1991, pp. 128-138.

15. Baldwin, B.; and Lomax, H.: Thin-Layer Approximation and Algebraic Model for Separated Turbulent Flows. AIAA Paper 78–257, Jan. 1978.

16. Chien, K.Y.: Predictions of Channel Flow and Boundary Layer Flow with Low Reynolds Number Turbulence Model. AIAA J., Vol. 20, No. 1, Jan. 1982, pp. 33–38.

17. Shuen, J.S.; and Yoon, S.: Numerical Study of Chemically Reacting Flows Using a Lower-Upper Symmetric Successive Overrelaxation Scheme. AIAA J., Vol. 27, Dec. 1989, pp. 1752–1760.

18. Yu, S.T.; Tsai, Y.-L. Peter; and Shuen, J.S.: Three-Dimensional Calculation of Supersonic Reacting Flows Using an LU Scheme, AIAA Paper 89–0391, Jan. 1989.

19. Yoon, S.; and Jameson, A.: An LU-SSOR Scheme for the Euler and Navier-Stokes Equations, AIAA Paper 0600, Jan. 1987.

20. Jameson, A.; and Yoon, S.: Lower-Upper Implicit Schemes with Multiple Grids for the Eulers Equations. AIAA J., Vol. 25, No. 7, July 1987, pp. 929–935.

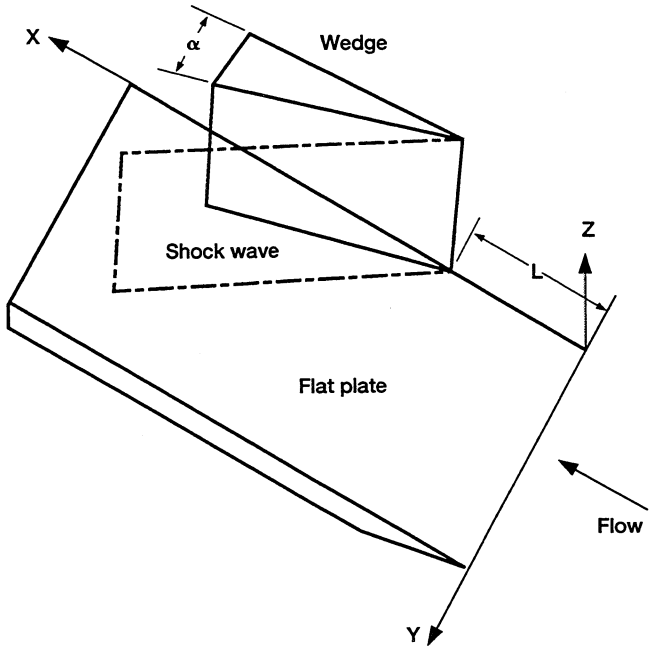

Figure 1.—Glancing shock wave over a flat plate boundary layer.

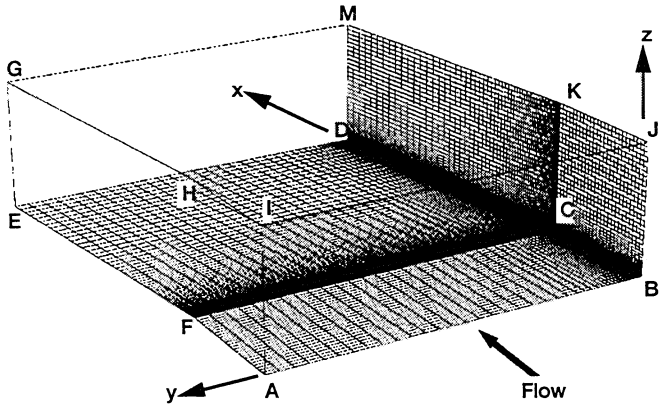

Figure 2.—Physical domain and grid system used in present study.

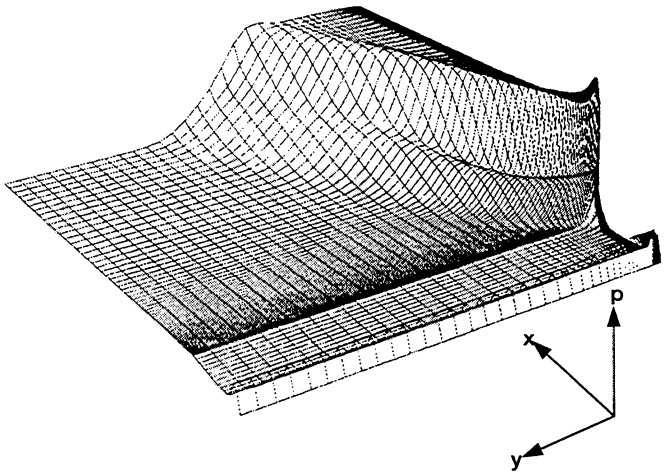

Figure 3.—Computed three-dimensional surface pressure distribution on the flat plate.

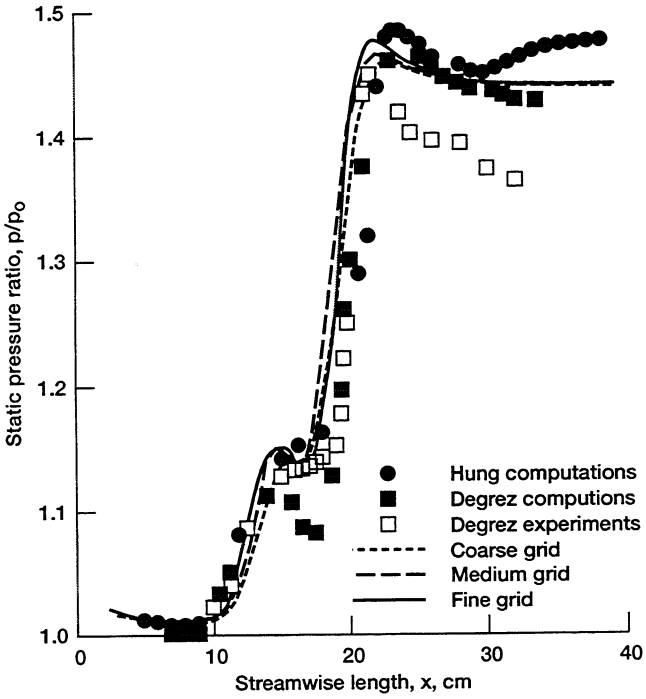

Figure 4.—Comparison of computed and experimental surface pressure distributions at y = 5 cm (M_o = 2.25; α = 6.0°; and Re_L = 1.08x10^5).

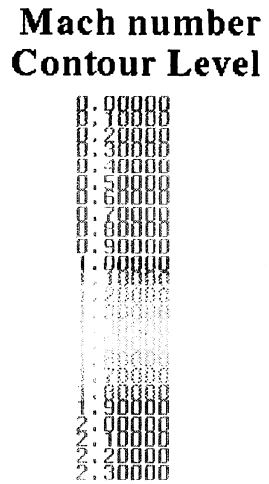

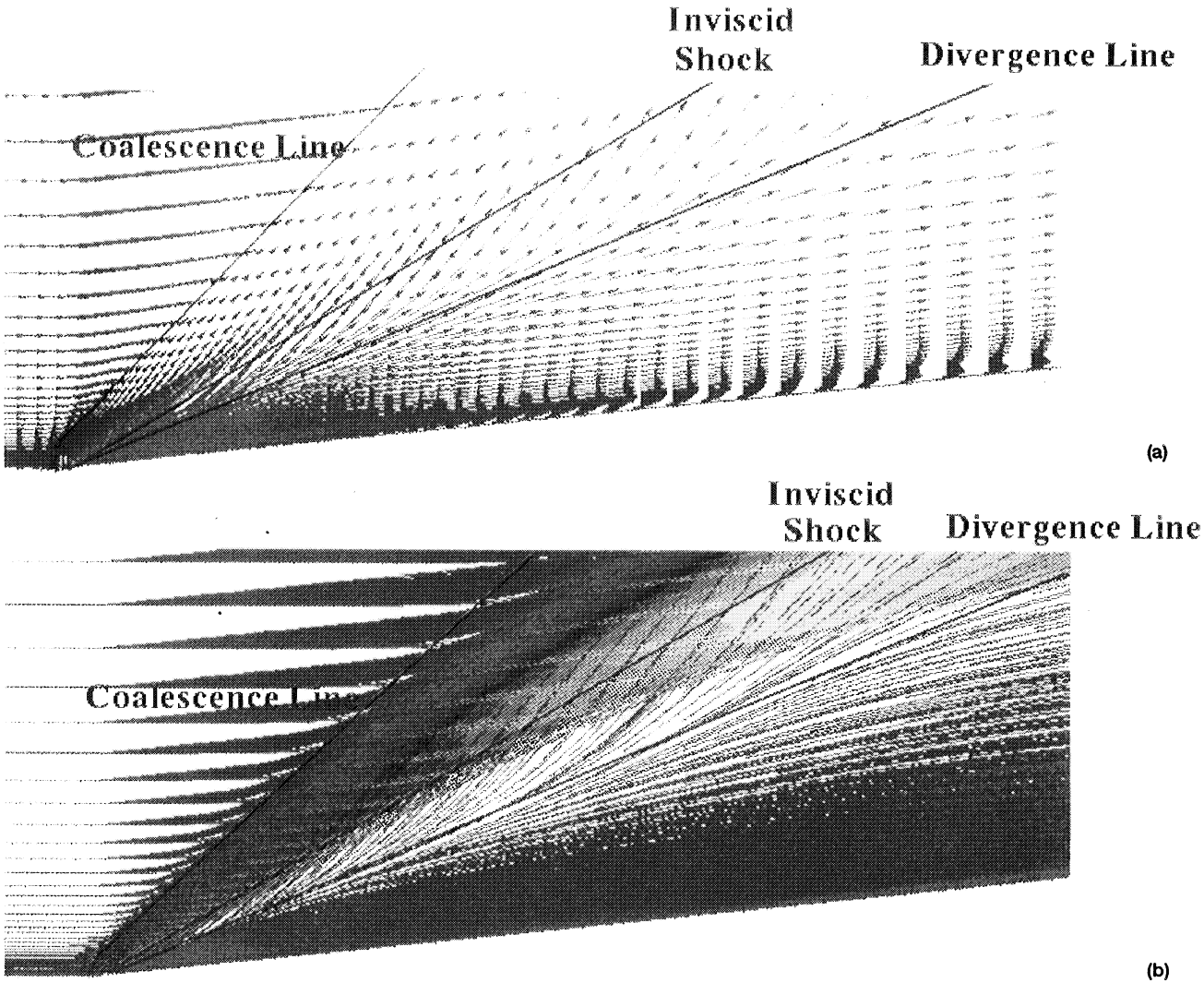

Figure 5.—Computed (a) velocity vectors and (b) particle traces on the flat plate for the laminar case.

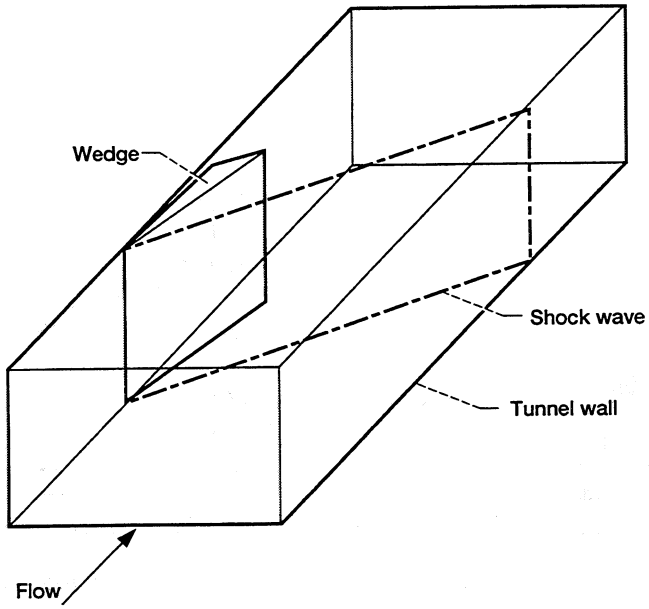

Figure 6.—Diagram of test configuration.

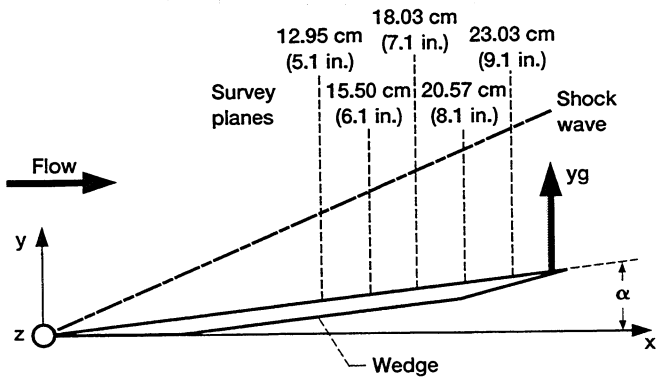

Figure 7.—Experimental survey locations.

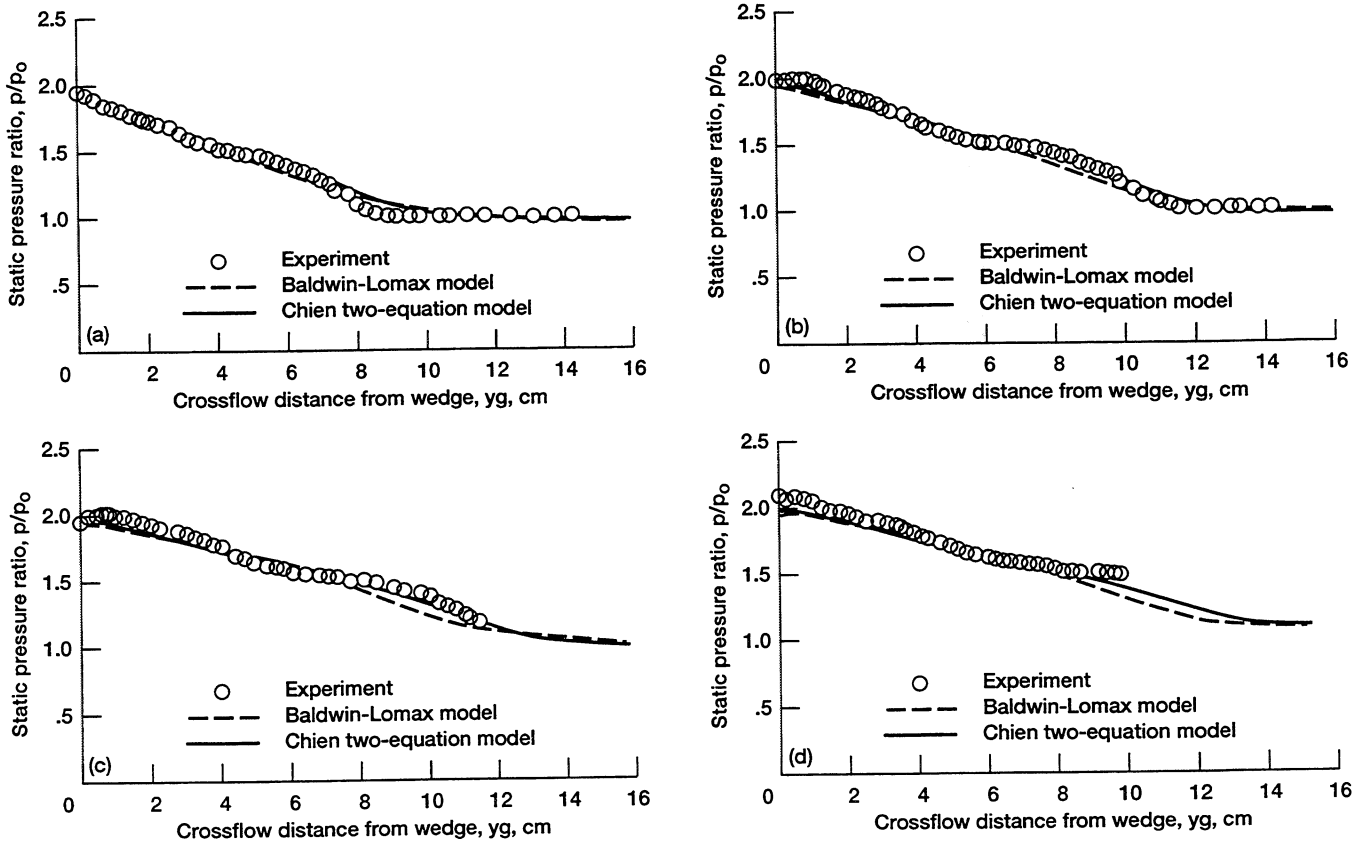

Figure 8.—Comparison of computed and experimentally determined static pressure distribution on a flat plate: (a) at x = 12.95 cm (5.1 in.); (b) at x = 18.03 cm (7.1 in.); (c) at x = 20.57 cm (8.1 in.); and (d) at x = 23.11 cm (9.1 in.).

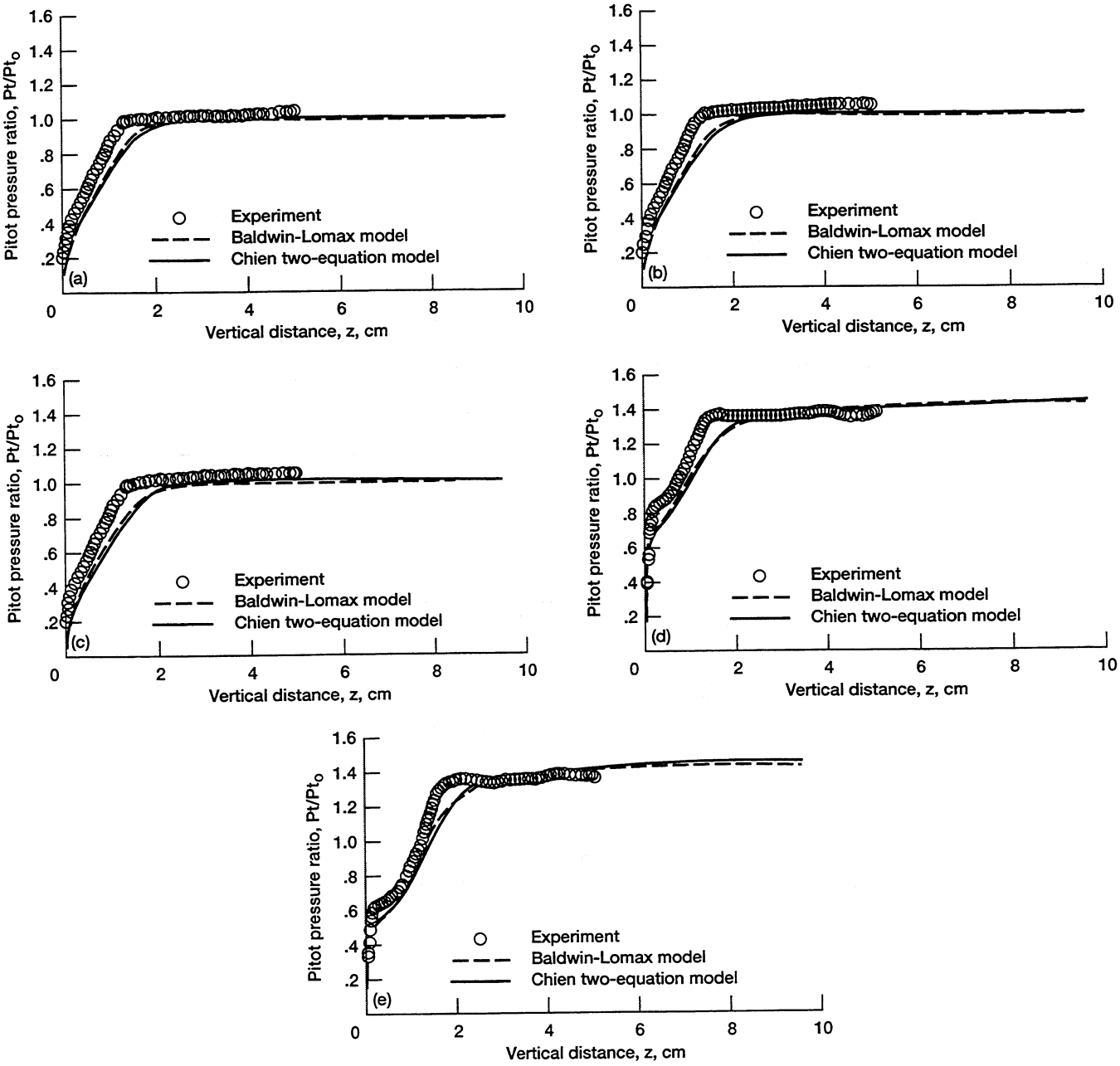

Figure 9.—Comparison of computed and experimentally determined pitot pressure distribution: (a) at x = 9.14 cm (3.6 in.) and yg = 6.07 cm (2.4 in.); (b) at x = 9.14 cm (3.6 in.) and yg = 7.37 cm (2.9 in.); (c) at x = 9.14 cm (3.6 in.) and yg = 9.91 cm (3.9 in.); (d) at x = 18.03 cm (7.1 in.) and yg = 1.91 cm (0.75 in.); and (e) at x = 18.03 cm (7.1 in.) and yg = 3.18 cm (1.25 in.).

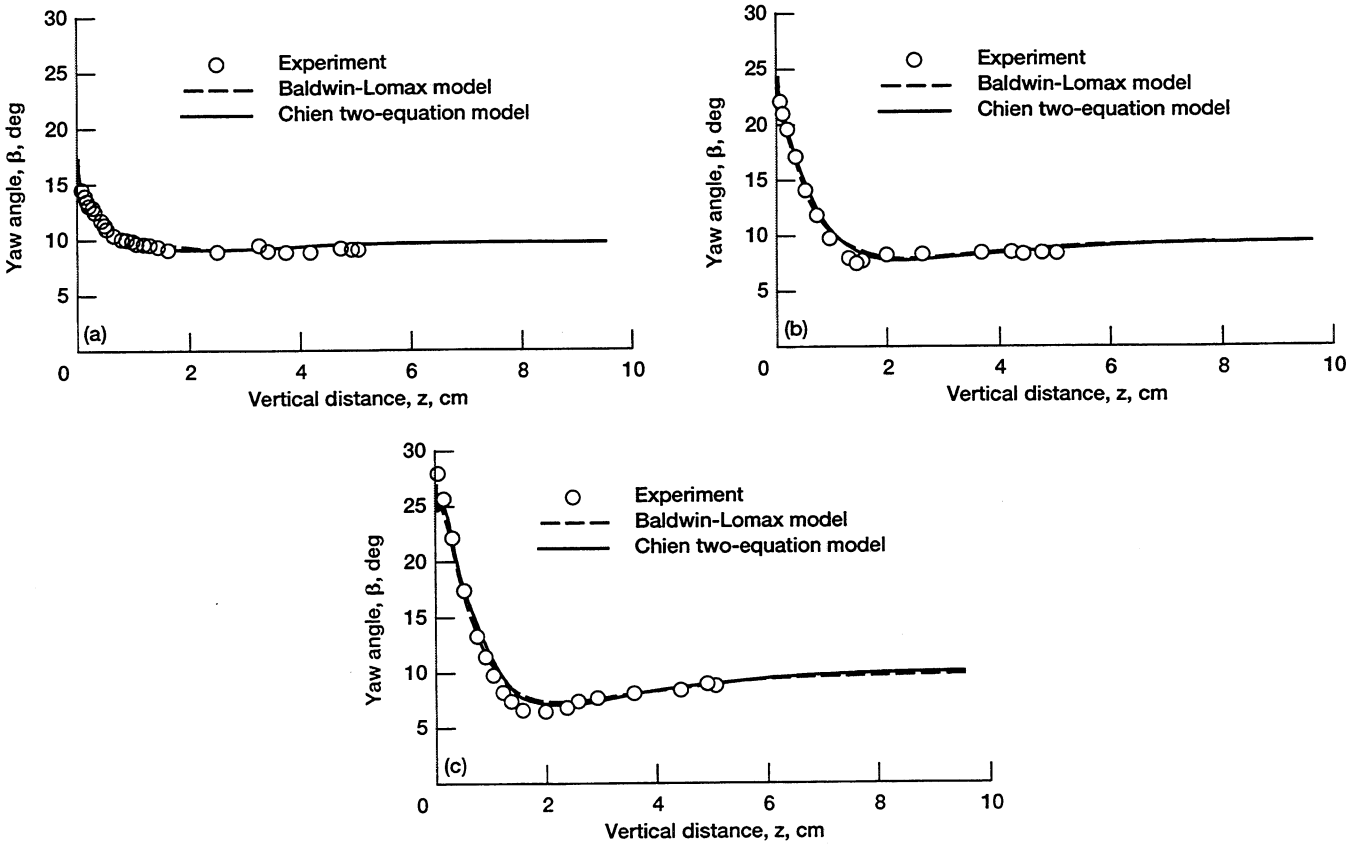

Figure 10.—Comparison of computed and experimentally determined yaw angle distribution for x = 18.03 cm (7.1 in.): (a) at yg = 0.64 cm (0.25 in.); (b) at yg = 1.91 cm (0.75 in.); and (c) at yg = 3.18 cm (1.25 in.).

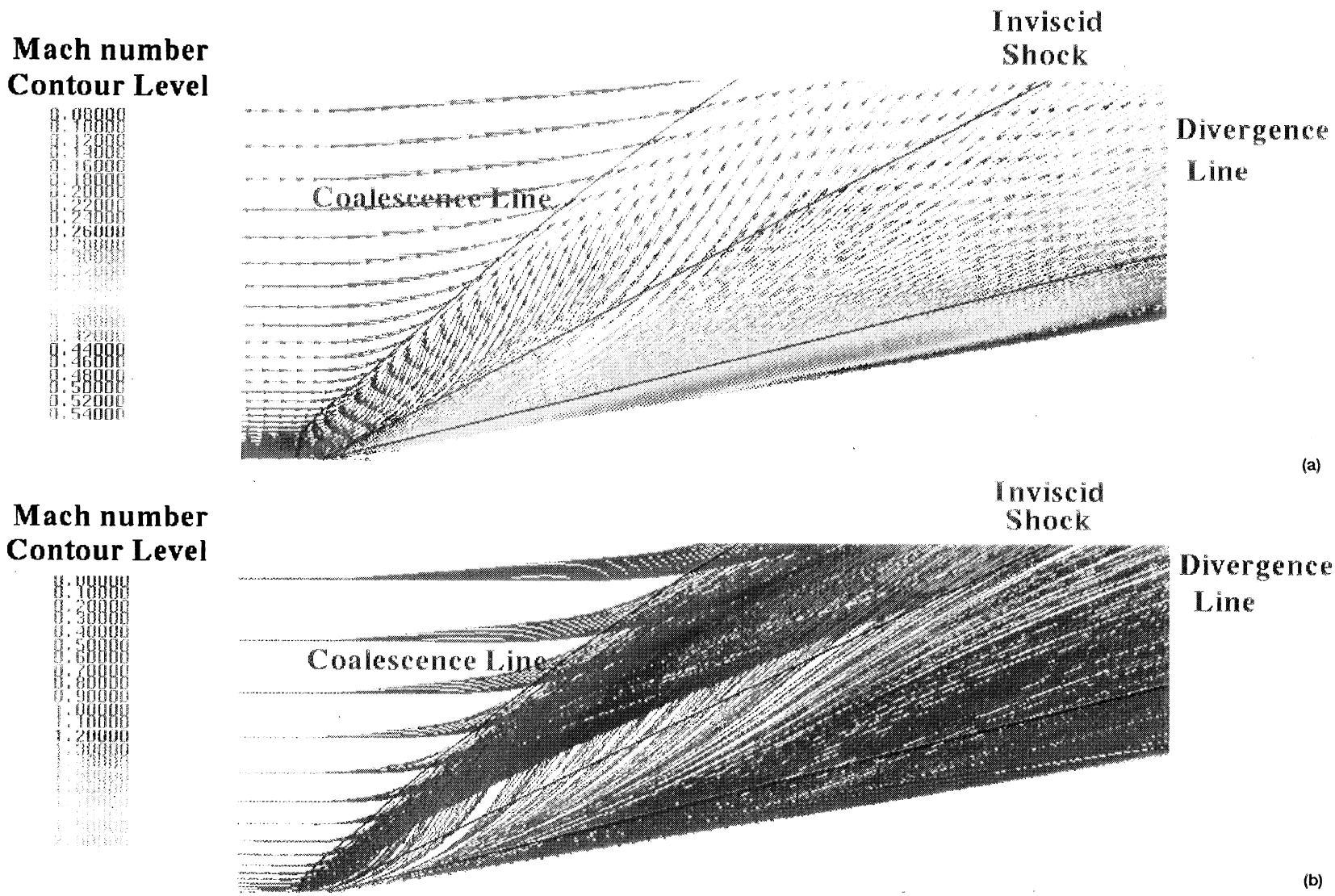

Figure 11.—Computed (a) velocity vectors and (b) particle traces on the flat plate for the turbulent case.

REPORT DOCUMENTATION PAGE

Form Approved
OMB No. 0704-0188

1. AGENCY USE ONLY (*Leave blank*)	2. REPORT DATE	3. REPORT TYPE AND DATES COVERED
	September 1994	Technical Memorandum

4. TITLE AND SUBTITLE

Validation of the RPLUS3D Code for Supersonic Inlet Applications Involving Three-Dimensional Shock Wave-Boundary Layer Interactions

5. FUNDING NUMBERS

WU–537–02–23

6. AUTHOR(S)

Kamlesh Kapoor, Bernhard H. Anderson, and Robert J. Shaw

7. PERFORMING ORGANIZATION NAME(S) AND ADDRESS(ES)

National Aeronautics and Space Administration
Lewis Research Center
Cleveland, Ohio 44135–3191

8. PERFORMING ORGANIZATION REPORT NUMBER

E–8839

9. SPONSORING/MONITORING AGENCY NAME(S) AND ADDRESS(ES)

National Aeronautics and Space Administration
Washington, D.C. 20546–0001

10. SPONSORING/MONITORING AGENCY REPORT NUMBER

NASA TM–106579

11. SUPPLEMENTARY NOTES

Bernhard H. Anderson and Robert J. Shaw, NASA Lewis Research Center; Kamlesh Kapoor, National Research Council–NASA Research Associate at Lewis Research Center. Responsible person, Kamlesh Kapoor, organization code 2780, (216) 433–8295.

12a. DISTRIBUTION/AVAILABILITY STATEMENT

Unclassified - Unlimited
Subject Category 02

12b. DISTRIBUTION CODE

13. ABSTRACT (*Maximum 200 words*)

A three-dimensional computational fluid dynamics code, RPLUS3D, which was developed for the reactive propulsive flows of ramjets and scramjets, was validated for glancing shock wave-boundary layer interactions. Both laminar and turbulent flows were studied. A supersonic flow over a wedge mounted on a flat plate was numerically simulated. For the laminar case, the static pressure distribution, velocity vectors, and particle traces on the flat plate were obtained. For turbulent flow, both the Baldwin-Lomax and Chien two-equation turbulent models were used. The static pressure distributions, pitot pressure, and yaw angle profiles were computed. In addition, the velocity vectors and particle traces on the flat plate were also obtained from the computed solution. Overall, the computed results for both laminar and turbulent cases compared very well with the experimentally obtained data.

14. SUBJECT TERMS

Shock wave; Boundary layer interactions

15. NUMBER OF PAGES

19

16. PRICE CODE

A03

17. SECURITY CLASSIFICATION OF REPORT	18. SECURITY CLASSIFICATION OF THIS PAGE	19. SECURITY CLASSIFICATION OF ABSTRACT	20. LIMITATION OF ABSTRACT
Unclassified	Unclassified	Unclassified	